Pergamon

Geochimica et Cosmochimica Acta, Vol. 68, No. 16, pp. 3351–3365, 2004

0016-7037/04 $30.00 + .00

doi:10.1016/j.gca.2004.02.016

Molecular modeling of water structure in nano-pores between brucite (001) surfaces

JIANWEI WANG,* ANDREY G. KALINICHEV, and R. JAMES KIRKPATRICK
Department of Geology, University of Illinois, 1301 W. Green St., Urbana, Illinois 61801 USA

(*Received August* 28, 2003; *accepted in revised form February* 18, 2004)

Abstract—Molecular dynamics (MD) computer simulations of liquid water held in one-dimensional nano-confinement by two parallel, electrostatically neutral but hydrophilic surfaces of brucite, $Mg(OH)_2$, provide greatly increased, atomistically detailed understanding of surface-related effects on the spatial variation in the structural ordering, hydrogen bond (H-bond) organization, and local density of H_2O molecules at this important model hydroxide surface. *NVT*-ensemble MD simulations (i.e., at constant number of atoms, volume and temperature) were performed for a series of model systems consisting of 3 to 30 Å-thick water layers (containing 35 to 360 H_2O molecules) confined between two 19 Å-thick brucite substrate layers. The results show that the hydrophilic substrate significantly influences the near-surface water structure, with both H-bond donation to the surface oxygen atoms and H-bond acceptance from the surface hydrogen atoms in the first surface layer of H_2O molecules playing key roles. Profiles of oxygen and hydrogen atomic density and H_2O dipole orientation show significant deviation from the corresponding structural properties of bulk water to distances as large as 15 Å (~5 molecular water layers) from the surface, with the local structural environment varying significantly with the distance from the surface. The water molecules in the first layer at about 2.45 Å from the surface have a two-dimensional hexagonal arrangement parallel to brucite layers, reflecting the brucite surface structure, have total nearest neighbor coordinations of 5 or 6, and are significantly limited in their position and orientation. The greatest degree of the tetrahedral (ice-like) ordering occurs at about 4 Å from the surface. The translational and orientational ordering of H_2O molecules in layers further from the surface become progressively more similar to those of bulk liquid water. A quantitative statistical analysis of the MD-generated instantaneous molecular configurations in terms of local density, molecular orientation, nearest neighbor coordination, and the structural details of the H-bonding network shows that the local structure of interfacial water at the brucite surface results from a combination of "hard wall" (geometric and confinement) effects, highly directional H-bonding, and thermal motion. This structure does not resemble that of bulk water at ambient conditions or at elevated or reduced temperature, but shares some similarities with that of water under higher pressure.

1. INTRODUCTION

Interaction between water and solid surfaces, and changes in their structural and dynamical behavior in the near-surface region can substantially affect the properties of both phases, including the reactivity and functionality of the near-surface region. These interactions are, thus, of significant interest in many geochemical, technological, and biologic systems. To adequately model and ultimately understand the interaction of aqueous solutions with rocks, sediments, soils, and other natural and synthetic materials where the aqueous phase is strongly perturbed by a surface, detailed knowledge of the structure and properties of interfacial water is essential (Hochella and White, 1990; Brown et al., 1999; Brown, 2001). It has also long been known that the dielectric and diffusive properties of water confined in nano-scale spaces are significantly different than these of bulk water (Packer, 1977; Nandi et al., 2000; Michot et al., 2002). Surface force (Israelachvili and Pashley, 1983; Israelachvili and Wennerström, 1996) and fluidity (viscosity) measurements of confined water (Raviv et al., 2001; Zhu and Granick, 2001) confirm such effects. The molecular-scale origins of these effects, however, are still not completely understood, despite significant recent experimental (Dore, 2000; Cheng et al., 2001; Teschke et al., 2001; Bellissent-Funel, 2002; Fouzri et al., 2002; Schlegel et al., 2002; Fenter et al., 2003) and computational (McCarthy et al., 1996; Bridgeman and Skipper, 1997; Spohr et al., 1999; Stöckelmann and Hentschke, 1999; Greathouse et al., 2000; Kalinichev et al., 2000; Park and Sposito, 2002; Sakuma et al., 2003) efforts to investigate the structure and dynamics of interfacial and nano-confined water. Most of these studies have focused on determining the differences between the properties of interfacial or confined water and bulk liquid water. For instance, atomic density variations, layering of water molecules (Lee and Rossky, 1994; McCarthy et al., 1996; Bridgeman and Skipper, 1997; Cheng et al., 2001; Park and Sposito, 2002; Schlegel et al., 2002; Fenter et al., 2003), and changes of diffusion coefficients (Lee and Rossky, 1994; Spohr et al., 1999; Greathouse et al., 2000; Kalinichev et al., 2000; Sakuma et al., 2003) near interfaces have been observed experimentally and in molecular dynamics (MD) simulations. However, effective prediction of how the structure, composition, and near-surface atomic charge distribution of the substrate affect the properties of water and their molecular scale origins remains elusive.

Molecular computational modeling has been highly effective in understanding the structure and properties of solids, bulk water, and aqueous solutions (e.g., Cygan, 2001; Kalinichev, 2001; Guillot, 2002), and has also made important contributions to understanding fluid-solid interfaces (Lee and Rossky,

* Author to whom correspondence should be addressed (jianwei7@uiuc.edu).

1994; McCarthy et al., 1996; Bridgeman and Skipper, 1997; Hartnig et al., 1998; Spohr et al., 1999; Stöckelmann and Hentschke, 1999; Gordillo and Martí, 2000; Greathouse et al., 2000; Kalinichev et al., 2000; Cygan, 2001; Gallo et al., 2002; Michot et al., 2002; Park and Sposito, 2002; Rustad et al., 2003). Here we present the results of a MD modeling study of the structure of water held in slit-like two-dimensional 3 to 30 Å-thick layers between two hydrophilic surfaces of the prototypical hydroxide phase brucite, $Mg(OH)_2$.

The surfaces of MgO and many other oxides are well-known to be hydroxylated in contact with water and at normal relative humidities (Refson et al., 1995; Liu et al., 1998; Brown et al., 1999), and thus, brucite is an important model material for many earth surface environments. It has a relatively simple layered structure containing single trioctahedral sheets with full Mg occupancy of the octahedral sites and fully vacant tetrahedral sites (Desgranges et al., 1996). The octahedral sheet has no permanent structural charge, and the interlayer is normally unoccupied.

A recent MD study of the mobility of H_2O molecules in an ~12.5 Å thick water slab confined between two (001) surfaces of brucite found, surprisingly, a factor of 1.5 increase of the self-diffusion coefficient and a factor of 0.8 decrease of the reorientation correlation time for near-surface molecules relative to bulk-liquid values (Sakuma et al., 2003). This result is in sharp contrast with many other MD simulation studies of similar aqueous interfaces that show *reduced* diffusion rates for water at the surfaces of hydroxylated crystalline silica (by a factor of ~5; Lee and Rossky, 1994), Vycor glass (at least by a factor of 10; Spohr et al., 1999), in the interlayer of smectite hydrates (by a factor of ~12; Greathouse et al., 2000), and in layered double hydroxides (by a factor of ~4; Kalinichev et al., 2000). Unfortunately, Sakuma et al. (2003) did not present sufficient detail about the structure of the interfacial water obtained in their simulations to allow effective comparisons to the simulations presented here.

In the present paper we focus on detailed quantitative analysis of the structure of near-surface water in terms of atomic density profiles, statistics of molecular orientations, two-dimensional radial distribution functions of H_2O within planes parallel to the surface, an order parameter quantifying the degree of tetrahedrality of the nearest neighbor molecular environments, and the structural details of the H-bonding network at the surface. Such structural understanding is essential to understanding and predicting the behavior and properties of near-surface fluids. Whenever possible, we compare our structural results with the data of Sakuma et al. (2003). Detailed analysis of the dynamics of H_2O molecules between brucite and other hydrophobic and hydrophilic mineral surfaces will be the subject of future work.

The structure of bulk liquid water, which is the reference state for near-surface water structure, is dominated by distorted tetrahedral local arrangements similar to those in the crystal structure of ice Ih (e.g., Eisenberg and Kauzmann, 1969; Soper, 2000; Errington and Debenedetti, 2001; Head-Gordon and Hura, 2002). In bulk liquid water, these local structural units compose an interconnected H-bonding network in which most H_2O molecules have four nearest neighbors. In ice Ih, each water molecule has exactly four nearest neighbors. Due to their mutual orientations, these molecules are able to donate two H-bonds and accept two others. In liquid water, the long range ice-like ordering is lost, and the ideal tetrahedral local H-bonding configuration is partially broken. An important component of this structural disruption is an increase in the number of so-called "interstitial" water molecules. These are fifth nearest neighbors to a given molecule but are not H-bonded to it (Eisenberg and Kauzmann, 1969; Bagchi et al., 1997; Kalinichev et al., 1999; Saitta and Datchi, 2003). Numerous experimental infrared, X-ray, and neutron scattering experiments and computational studies provide a quite consistent picture of the local structure of water at ambient conditions. The differences are mainly due to different criteria to define hydrogen bonding by various experimental techniques, and differences in the interatomic potential used in the computations (e.g., Gorbaty and Kalinichev, 1995; Kalinichev, 2001; Head-Gordon and Hura, 2002). These studies show that a water molecule in bulk liquid has on average 4.4 to 5.2 nearest neighbors and participates in 3.2 to 3.9 H-bonds. Here we show that H-bonding to hydroxide surfaces can produce an interfacial water structure different in many respects from those of bulk water or any known ice phase.

The presence of a surface is well known to perturb the fluid structure and properties up to several molecular diameters from the surface (Israelachvili and Pashley, 1983; Michot et al., 2002). The interactions that cause these perturbations are especially complicated for molecules like water that have small molecular diameters and large dipole moments. For simple cases such as a hard sphere fluid at a hard wall, or a Lennard-Jones fluid such as argon at a Lennard-Jones surface, the "hard wall" effects dominate (Abraham, 1978). The density variation perpendicular to the surface oscillates with a periodicity equal to the molecular diameter (Abraham, 1978; Yu et al., 1999). For water at most surfaces, however, H-bonding and electrostatic interactions complicate this simple picture. The ability of a surface to participate in an H-bonding network is expected to play a key role in defining the local structure and dynamics of water molecules in confined spaces and at interfaces. Thus, the structure of water in an interfacial region results from a balance of the ordering due to H-bonding, "hard wall" effects, and disordering due to thermal motion. It is well known that H-bonding is responsible for the anomalous behavior of many properties of water, such as the density maximum at 4°C (e.g., Geiger and Stanley, 1982; Poole et al., 1994).

Surfaces with different compositions and different local atomic charge distributions, even on an otherwise neutral surface, are expected to have greatly different substrate-specific effects on the structure of interfacial water. For instance, molecular modeling shows that at the (001) surface of mica and other sheet silicates, water molecules are adsorbed onto the ditrigonal cavities above the six-member rings formed by SiO_4 tetrahedra (Bridgeman and Skipper, 1997; Smirnov and Bougeard, 1999; Greathouse et al., 2000; Park and Sposito, 2002). Neutron diffraction studies of water confined in silica gel and the pores of Vycor glass suggest that the water structure is similar to that of bulk water at temperatures ~30° lower than the experimental temperature (Dore, 2000; Bellissent-Funel, 2001). MD simulations of water molecules confined in carbon nanotubes (Gordillo and Martí, 2000) show fewer H-bonds than in bulk water. For water confined in silica pores with all nonbridging oxygens saturated with acidic hydrogens, com-

puter simulations demonstrate that the H-bonding network is largely destroyed near the surface but is restored again at distances beyond ~4 Å from surface (Gallo et al., 2002). The structure and dynamics of interlayer water, a special case of confined water in which H_2O molecules are usefully thought of as part of the crystal structure, have been investigated by many recent experimental and computational studies (Kagunya, 1996; Smirnov and Bougeard, 1999; Greathouse et al., 2000; Kalinichev et al., 2000; Wang et al., 2001; Wang et al., 2003). These results show that interlayer water is normally much more ordered than bulk liquid water, that the structure and composition of the basal surface plays a dominant role in determining the water structure, and that the diffusion rates are reduced by up to two orders of magnitude.

2. MATERIAL AND METHODS

2.1. Model Structures

The brucite crystal structure (trigonal, $P\bar{3}m1$) used as the basis for the simulations presented here was determined by neutron diffraction measurements (Desgranges et al., 1996). The MD simulations of the bulk crystal reproduce this structure well, yielding unit cell dimensions within 0.1% of the experimental values for the *a* and *b* dimensions ($a_{exp} = b_{exp} = 3.148 \pm 0.001$Å, $a_{calc} = b_{calc} = 3.15 \pm 0.01$Å) and 5% for the *c* dimension ($c_{exp} = 4.779 \pm 0.002$Å, $c_{calc} = 4.55 \pm 0.02$Å). The resulting calculated unit cell angles, $\alpha = 89.85^o \pm 0.37^o$, $\beta = 90.12^o \pm 0.29^o$, $\gamma = 119.98^o \pm 0.22^o$ are in good agreement with the observed trigonal symmetry (Desgranges et al., 1996). This agreement is expected because the brucite structure was one of the input phases originally used for the CLAYFF force field parameterization (Cygan et al., 2004).

The calculations show the OH groups to be, on average, perpendicular to the octahedral sheet, with the H atoms having broader distributions around their average positions than other atoms, in agreement with their large measured anisotropic thermal parameters (Desgranges et al., 1996). The MD results also confirm that bifurcated and even trifurcated H-bonds, (in which one H atom is simultaneously H-bonded to two or three neighboring O atoms) are present between two hydroxide layers (Desgranges et al., 1996). The computed positions of H-atoms in the brucite structure show a triangularly shaped distribution of atomic density that indicates dynamic disorder among three statistically equivalent sites. This is in qualitative agreement with the "three-site split-atom" model of Desgranges et al. (1996), where the position of each H atom is statistically split between three equally occupied sites, and the O-H direction is tilted toward nearest O-of-OH, making an angle with the threefold axis of ~9° at room temperature.

$Mg(OH)_2$ surfaces were created by cleaving the model crystal structure at the center of an interlayer parallel to (001) with all OH groups remaining intact. Six different models with empty, slit-like pore spaces were created by increasing the crystallographic *c* dimension of the simulation cells by 3.0, 6.0, 9.0, 12.0, 15.0, and 30.0 Å at the position of the cleavage (all model systems will be referred to by these values in the following discussion). Volumes of liquid water with a density of 1.0 g/cm^3 and the same size and shape as the empty pore spaces were prepared and then inserted in the empty pores. The combined water-brucite systems had P1 symmetry and the same crystallographic parameters as brucite, except for the *c* dimension. Each simulation supercell consisted of (6 × 6 × 4) crystallographic unit cells of brucite. These cells contained 144 Mg atoms and 288 OH groups and had dimensions of 18.78 Å × 18.78 Å × 21.09–52.59 Å in the *a*-, *b*-, and *c*-directions respectively, depending on the width of the pore. The number of water molecules varied from 35 to 360 (Fig. 1). We assume a uniform fully hydroxylated surface and applied no charge redistribution to the surface OH-groups. This surface model is assumed to approximate the conditions near the zero point of net proton charge (ZPNPC). Generally, the protonation state of a brucite surface in contact with water may be different than that of a cleaved surface if the pH is different from the ZPNPC. The ZPNPC of brucite is not known, but protonation and deprotonation reactions are well known to occur at hydroxide surfaces (Drever, 1997; Rustad et al., 2003).

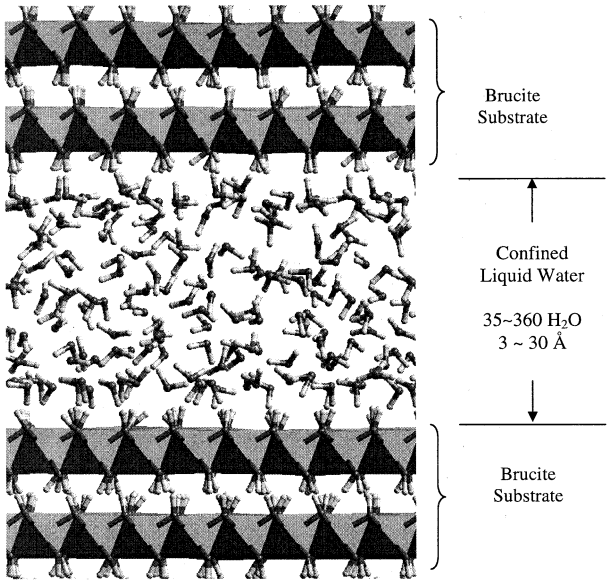

Fig. 1. Illustration of the models for water confined between brucite (001) surfaces. The V-shaped objects are water molecules, the octahedral sheets are the brucite, and the sticks attached to the octahedra are the O-H bonds of OH-groups. See text for a description of the models used.

2.2. MD Simulations

The simulations described here use the recently developed CLAYFF force field (Cygan et al., 2004), which has already proven to be highly effective in modeling the structures of many oxide, hydroxide, clay, and cement phases; the interaction of aqueous solutions and their dissolved species with mineral surfaces; and the behavior of interlayer ions and water (Kalinichev et al., 2000; Cygan, 2001; Wang et al., 2001; Kalinichev and Kirkpatrick, 2002; Kirkpatrick et al., 2003; Wang et al., 2003). CLAYFF is specifically optimized based on the observed structures of simple well-characterized oxides, hydroxides, and oxyhydroxides (Cygan et al., 2004). In this force field, the partial atomic charges are derived from periodic density functional theory (DFT) quantum calculations for these model compounds, and the non-Coulomb interactions are described by the conventional Lennard-Jones (12–6) function. Thus, the energy expressions for brucite are:

$$E_{Coulomb} = q_i q_j / 4\pi\varepsilon_0 r_{ij} \quad (1)$$

$$E_{vdW} = D_{0,ij}[(R_{0,ij}/r_{ij})^{12} - 2(R_{0,ij}/r_{ij})^6], \quad (2)$$

where for Mg, $D_{0,i} = 9.03$E-07 kcal/mol, $R_{0,i} = 5.91$ Å, and $q_i = 1.36e$, for O of OH, $D_{0,i} = 0.1554$ kcal/mol, $R_{0,i} = 3.55$ Å and $q_i = -1.105e$, and for H of OH, $q_i = 0.425e$. The parameters of unlike interactions are calculated according to the arithmetic mean rule for the distance parameter, R_0, $R_{0,ij} = (R_{0,i} + R_{0,j})/2$, and the geometric mean rule for the energetic parameter, D_0, $D_{0,ij} = \sqrt{D_{0,i} D_{0,j}}$. ε_0 is the dielectric permittivity in vacuum ($\varepsilon_0 = 8.85419 \times 10^{-12}$F/m).

For water molecules, we use the flexible version of the simple point charge (SPC) potential (Berendsen et al., 1981; Teleman et al., 1987). The SPC water model has partial charges centered directly on each of three atoms, and the short-range interactions are represented by one Lennard-Jones term centered on the oxygen atom. It is one of the most comprehensively tested models for water, and it has been used widely in molecular modeling of aqueous systems for the past two decades. Despite its relative simplicity, the SPC model successfully reproduces many properties of water, including structure, atom-atom radial distribution functions, and hydrogen bonding characteristics (e.g., Jorgensen

et al., 1983). Numerous simulations of aqueous systems with different water potentials have demonstrated that many of these results are quite robust in the sense that qualitatively they are not potential dependent (e.g., Kalinichev, 2001; Guillot, 2002). Thus, we expect the structural interpretations of the simulations presented here to not be critically dependent on the water potential used, and to be generally applicable.

The MD simulations were performed using periodic boundary conditions in all three crystallographic directions. Ewald summation to calculate long-range electrostatic contributions to the potential energy and a "spline cutoff" method to calculate short-range van der Waals interactions were used (e.g., Allen and Tildesley, 1987). Two stages of relaxation were applied to the initial six models. First, the positions of all atoms in the brucite substrate were fixed, and only the confined liquid water subsystem was allowed to relax under energy minimization and in relatively short (10–50 ps) *NVT*-ensemble MD runs. Then all atoms of the system were allowed to relax under similar conditions. The total energy of each model converged to a minimum within 0.001 kcal/mol, and these optimized structures were then used as the starting configurations for *NVT*-ensemble MD simulations at 300 K. A time step of 1.0 fs was used for all MD simulations, and each system was allowed to equilibrate for 100 to 500 ps of MD simulation depending on its size. To ensure thermodynamic equilibrium, the convergence of the total energy, its components, temperature, pressure, and the atomic radial distribution functions were carefully monitored during the equilibration period. The equilibrium dynamic trajectory for each model was finally recorded for statistical analysis at 10 fs intervals during the next 500 ps of MD simulation.

2.3. Simulation Analysis

Atomic density profiles in the [001] direction perpendicular to the solid surface were calculated by averaging over the 50000 frames of the 500 ps equilibrium MD trajectories for each system. The planes defined by the average positions of the surface oxygen atoms of brucite were taken as the origin ($z = 0$). Atomic density maps, time-averaged over instantaneous positions of specific atom types along the trajectory and projected onto the (001) plane, were also computed for each atom type in the system at various locations from the surface and for various layer thickness (Kalinichev and Kirkpatrick, 2002).

The directions of the three vectors describing the instantaneous orientation of each water molecule, the dipole vector ($\mathbf{v}_D$, parallel to the bisector of the H-O-H angle), the H-H vector ($\mathbf{v}_{HH}$) from one hydrogen atom to the other, and the normal ($\mathbf{v}_N$) to the H-O-H plane, were defined by the angles (φ_D, φ_{HH}, and φ_N, respectively) between the vectors and the [001] direction (normal to the surface) of the model brucite structure. The orientations were computed for each H_2O molecule at each time step, and the distributions of these angles were calculated as functions of distance from the brucite surface.

The topology of the water structure was quantitatively characterized by calculating two- and three-dimensional radial distribution functions (RDFs), parameters related to the instantaneous number of H-bonds donated and accepted by each individual water molecule, and the orientational order parameter (Errington and Debenedetti, 2001). RDFs give the probability of finding a pair of atoms, *i* and *j*, a distance *r* apart, relative to the probability expected for a random distribution of atoms at the same density. Three-dimensional O-O, O-H, and H-H RDFs for H_2O were computed, and nearest neighbor coordination numbers were calculated by integrating the RDF to the first minimum. In addition, two-dimensional RDFs were calculated for the atoms located in 0.2 Å thick slices parallel to the surface and as functions of distance from the surface. These RDFs reflect only correlations among atoms within these slices. To calculate the oxygen-oxygen and oxygen-hydrogen nearest neighbor (NN) coordination numbers, the cutoff distances of 3.3 Å and 2.45 Å were used, respectively, because these distances correspond to the first minima in their respective RDFs in bulk water (e.g., Jorgensen et al., 1983; Kalinichev, 2001).

The local organization of the H-bonding network is described by calculated values for the total number of H-bonds (HBs) per water molecule, the number of H-bonds donated to and accepted from other H_2O molecules, the number of H-bonds donated to and accepted from surface OH groups, and the fraction of water molecules with different numbers of H-bonds (distribution of H-bonding states). These parameters were calculated as the average over the computed trajectory as functions of distance from the surfaces. The criteria for the existence of an H-bond used here are those often used for bulk liquid water: intermolecular O•••H distances less than 2.45 Å and angles, β, between O•••O and O-H less than 30° (e.g., Luzar, 2000; see Fig. 2). Surface OH groups are treated in the same way as OH of water molecules for the purpose of HB calculations. The threshold of $R_{O\cdots H} = 2.45$ Å was used because it corresponds to the first minimum of the O-H radial distribution function for SPC water at ambient conditions, while $\beta \leq 30°$ covers 90% of the angular distribution of H-bonds in water under the same conditions (e.g., Teixeira et al., 1990; Luzar, 2000).

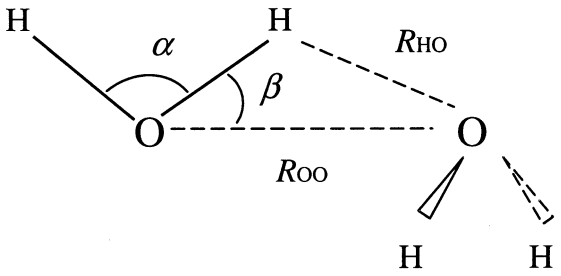

Fig. 2. Illustration of the parameters used in defining H-bonds in this study. H-bonds must simultaneously have intermolecular O•••H distances, *R*OH, less than 2.45 Å and angles, β, between O•••O and OH less than 30.0°. Surface OH groups are treated in the same way as OH of water molecules for this purpose.

The orientational order parameter, *q*, is an effective measure of the deviation of the local short-range water structure from the ideal tetrahedrality observed in crystal ice Ih. It is given by the expression:

$$q = 1 - \frac{3}{8}\sum_{j=1}^{3}\sum_{k=j+1}^{4}\left(\cos\psi_{jk} + \frac{1}{3}\right)^2, \qquad (3)$$

where ψ_{jk} are the angles formed by the lines connecting the O atom of the central H_2O molecule with any two of the four nearest neighbors, *j* and *k* ($j,k \leq 4$) (Chau and Hardwick, 1998; Errington and Debenedetti, 2001). The values of *q* vary from 1 for the ideal structure of ice Ih to 0 for a completely disordered state (e.g., ideal gas). This definition, originally introduced for the analysis of bulk water (Chau and Hardwick, 1998), was modified here to analyze the orientational ordering of interfacial water molecules by including surface OH groups into the calculation of the ψ_{jk} angles in additions to H_2O molecules.

3. RESULTS AND DISCUSSION

3.1. Density Profiles and H_2O Orientations

The density profiles for oxygen and hydrogen atoms and the orientational profiles for H_2O molecules are symmetrical on either side of the water layer and provide the basis for understanding the effects of confinement and the hydroxide surface structure on the interfacial water (Figs. 3, 4 and 5). For confined water layers 15 Å-thick and greater, the O-profiles exhibit four peaks at ~2.45, 5.05, 6.25, and 9.05Å, and smaller variations up to 15 Å from the surface. The H-profiles for the same systems have three peaks at 1.42, 2.83, and 5.50 Å, with no significant variation at distances greater than ~10 Å from the surface. For thinner pores, the structure of the entire water volume is substantially perturbed compared to bulk water, and the effects of the surface depend significantly on pore thickness (Fig. 3). For instance, the second O-peak is weaker in the 6 Å system than in the 9 Å system, and its position is at 3.7 Å from the surface in the 6 Å system compared to 5.0 Å in the 9 Å system. Similarly, the fourth maximum at ~9.30 Å in the 15 Å

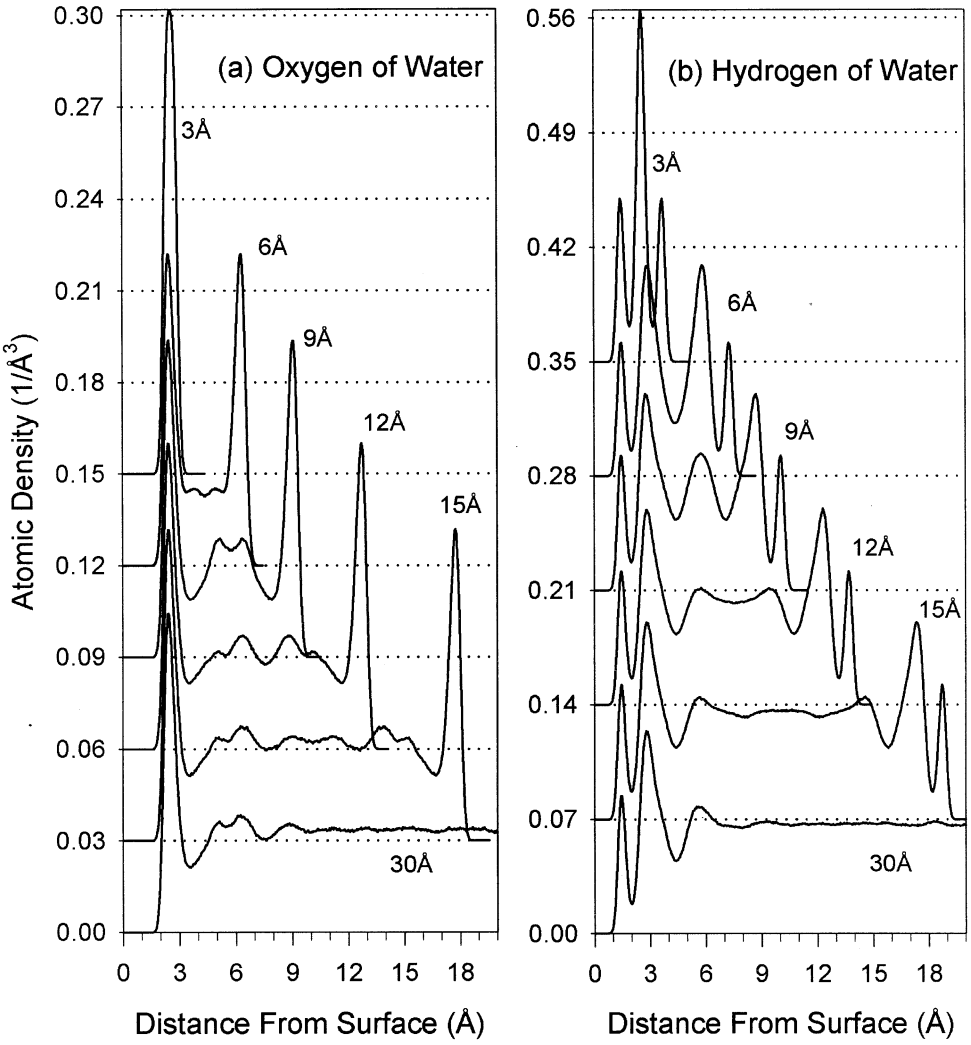

Fig. 3. Computed atomic density profiles for water confined between brucite layers. Curves are displaced vertically by 0.03 Å^{-3} (oxygen atomic density) and 0.07 Å^{-3} (hydrogen atomic density) to avoid overlap. The position of the surface (0.0 in these plots) is computed as the average position of the brucite surface oxygen atoms. The system size labels are the increases the brucite *c*-axis dimension used to generate the systems; the actual water layer thicknesses vary somewhat from these values. See text for details.

system shifts to 9.05 Å in the 30 Å system (Fig. 3). The distances between maxima in the O-density profiles are not equally spaced, as would be expected from hard wall effects alone. Thus, the surface structure, atomic charge distribution on the nominally neutral surface, and hydrogen bonding must play important roles in controlling the near surface water structure.

A unique interpretation of the water structure and the origin of the correlations between the O-and H-profiles is not possible from the density profiles alone or from these profiles combined with only averaged molecular orientations (Lee and Rossky, 1994; Bridgeman and Skipper, 1997). Here, the variation of the H_2O orientational distributions with distance from the surface provides useful insight (Figs. 4 and 5). In interpreting these figures, it is important to note that the angular distributions of the dipole vector (φ_D) as shown in Figure 4 have an inversion point at their center because of the sign convention related to defining the orientations with respect to the surface normal [001]. In contrast, the distributions of the H-H vectors (φ_{HH}), shown only in Figure 5, are symmetric with respect to 90° because of the arbitrary choices of the initial vector directions for all water molecules in each frame and their orientational changes over time. The results show that for water layer thickness of less than 12 Å, the orientations of all molecules are strongly affected by the presence of the surface, although the effect is less at distances >6 Å. Only in systems 12 Å and larger does the angular distribution in the middle of the pore approach the *sin(φ)* distribution expected for the angle φ between a randomly oriented vector and an arbitrary axis (in this case [001]). As illustrated by the dipole orientation distributions in Figure 4, the features of the distributions that occur in the thin pores also occur in the larger ones, although their positions and magnitudes are not identical. These results parallel the results for the atomic density distributions.

The orientational distribution of water molecules contributing to the first peak in the O-density profiles (Fig. 3) has two components that dominate at different distances from the sur-

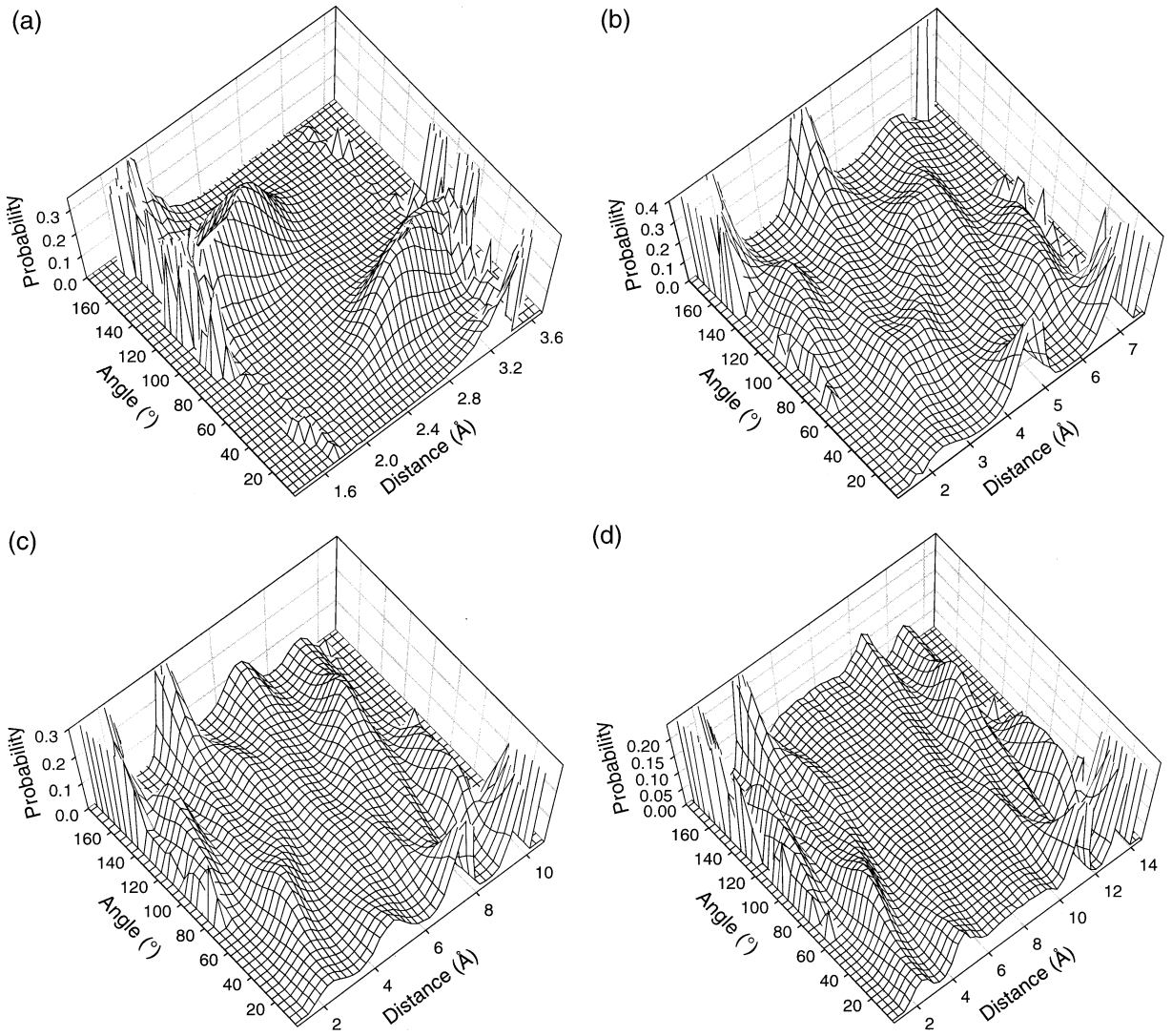

Fig. 4. The angular distributions of the H_2O dipole vector with the distance from brucite surface for confined water molecules. The angle is defined between the dipole vector and [001] direction. The probabilities were first normalized by a sinusoid distribution and then normalized by the total number of water molecules at the distances indicated. Thus, the integrals of each curve at any given distance from surface are equal. (a) 3 Å system; (b) 6 Å system; (c) 9 Å system; and (d) 12 Å system.

face, indicating multiple minima in the near-surface potential energy surface (PES). These two orientations are the result of two different H-bonding configurations for water molecules at the surface. Type-1 molecules are, on average, slightly closer to the surface (mean distance ~2.3Å) and are predominantly oriented with $\varphi_D \sim 130°$, $\varphi_{HH} \sim 0-45°$, and $\varphi_N \sim 50-90°$ (dipole axis tilted toward the surface). One H-atom of these water molecules lies close to the surface and contributes to the first peak in the H-density profile at 1.42 Å, and the other H-atom contributes to the second peak at 2.80 Å. Type-2 molecules are, on average, somewhat further from the surface (~2.6Å), and are predominantly oriented with $\varphi_D \sim 30-80°$, $\varphi_{HH} \sim 40-90$, and $\varphi_N \sim 10-40°$ (dipole axis tilted away from the surface). Both H-atoms of these molecules contribute principally to the second peak in the hydrogen density profile. Figure 6 schematically illustrates the most probable orientations of these two types of first-layer molecules, along with those of others further from the surface. The ratio of type-1 to type-2 molecules is ~5/4, as estimated by counting the number of molecules with up-pointing and down-pointing dipoles and from the volumes under the peaks in the un-normalized orientation distribution profiles (data not shown). The recent MD simulation of water at the brucite (001) surface by Sakuma et al. (2003) also identified two types of water molecules comparable to those found here. In their simulations, one type has on average $\varphi_D = 120°$ and $\varphi_N = 90°$, and the other $\varphi_D = 50°$ and $\varphi_N = 45°$.

Water molecules with these two different orientations are intimately mixed with each other in the plane parallel to the surface, and there are no clear correlations of their occurrence near each other. Large domains of one structural type cannot form because the H-bond formation between neighboring water molecules prevents each type of environment

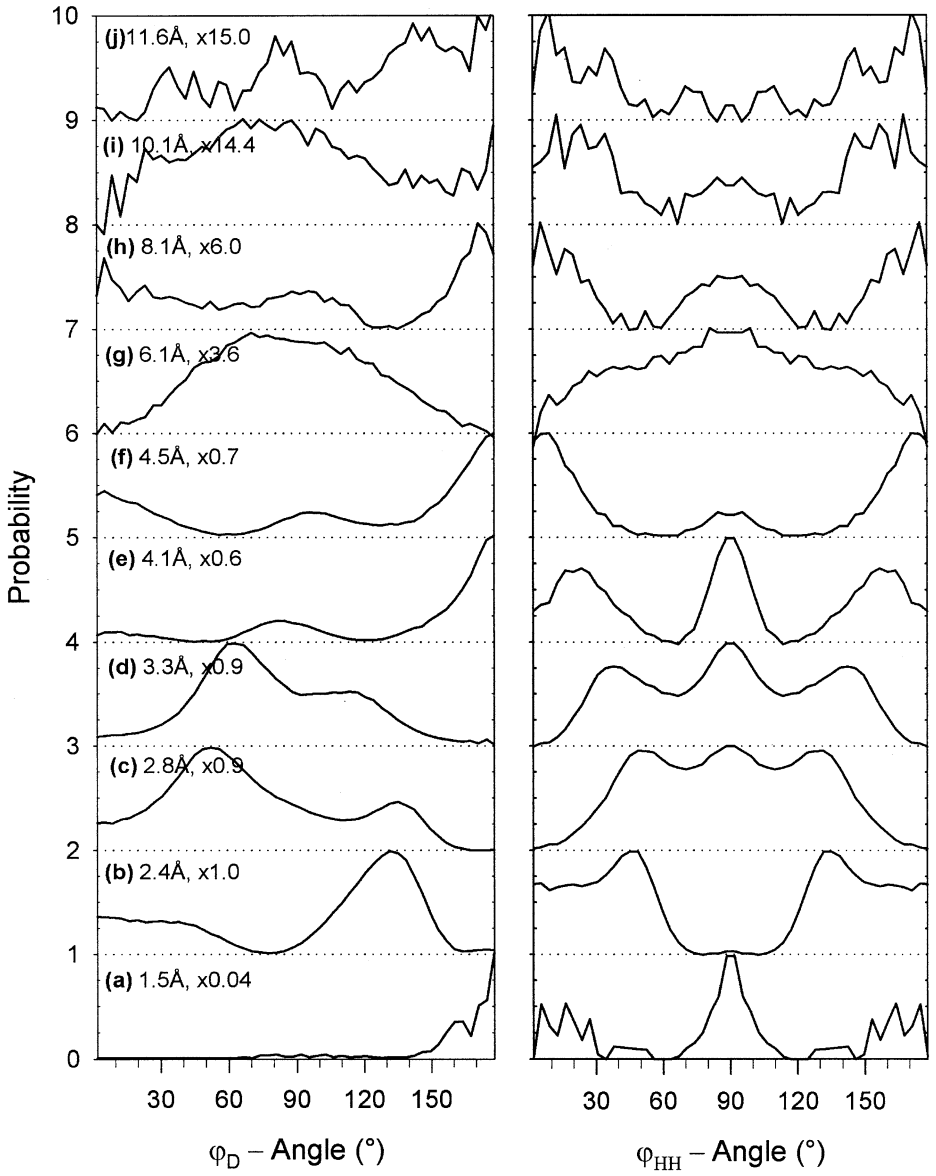

Fig. 5. The angular distributions of the water orientations in the 30 Å system. φ_D (left) and φ_{HH} (right), are angles between the water dipole and [001], and between the water H-H vector and [001] respectively. Each curve was normalized as in Figure 4 and rescaled individually and displaced vertically by 1.0 to fit the figure. The values listed in Fig. (a) to (j) are the distances from the surface.

from extending more than 3 molecules in the plane parallel to the surface.

In addition, our simulations also show a small fraction of water molecules located at distances less than 1.8 Å from the surface. These molecules have dipole orientations of approximately 180° to the surface normal (both H-atoms oriented towards the surface) and donate 2 H-bonds to surface OH groups. The number of molecules with this configuration is very small (<0.005 water per surface OH group) (Fig. 3), and visualization of the MD trajectories shows that these molecules retain their orientations for only tens of femtoseconds. This is comparable to the time for proton transfer in liquid water (Geissler et al., 2001). Whether the presence of molecules with this orientation is indicative of proton transfer between the water molecules and surface OH groups cannot be addressed by classical MD methods, and would require an ab initio molecular dynamics approach.

Previously published MD simulations for water at a variety of oxide and hydroxide surfaces also show the presence of molecules with two different orientations in the first layer, although the local structural environments or orientations are slightly different for each phase. The coexistence of water molecules with different orientations, but mixed and interconnected in the plane parallel to the surface, appears to allow the development of an interconnected H-bond network involving the water molecules and surface atoms. For all oxide and hydroxide surfaces so far studied, the orientations of the water molecules in the first near-surface layer are restricted to sub-

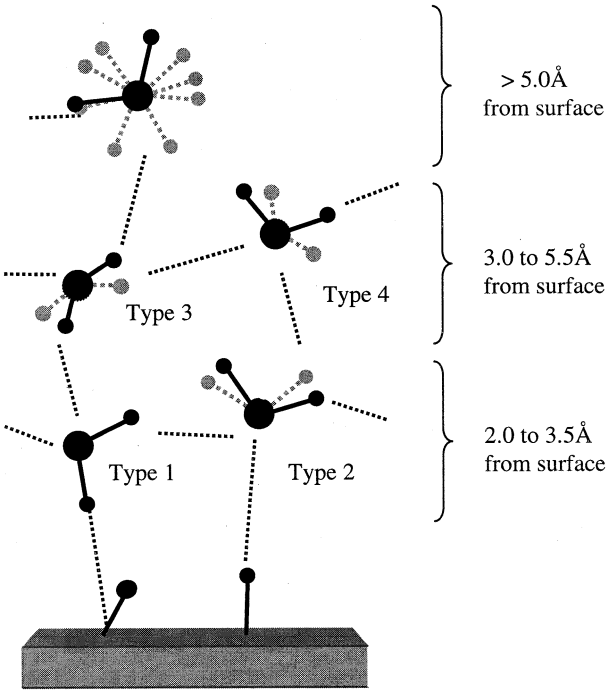

Fig. 6. Schematic diagram illustrating the orientations and H-bonding of water molecules in the different near-surface layers defined in the text. Black balls and sticks are water molecules or surface OH groups. Dotted balls and sticks are water molecules with different orientations that schematically show orientational ranges in the different layers. The dotted lines connecting water molecules are H-bonds.

strate-specific, but relatively narrow angular ranges, indicating a significant reduction in their orientational mobility relative to bulk water. At the MgO (001) surface, the H_2O dipoles in the first molecular layer of water occur predominantly at φ_D = 107° and 60° (McCarthy et al., 1996), corresponding, respectively, to orientations in which the H_2O molecules donate H-bonds to the surface oxygen, and the orientations where H_2O molecules are only H-bonded to other H_2O molecules but not to the surface. At talc surfaces, water dipoles have two predominant lowest-energy orientations corresponding, in our notation, to φ_D = at 0° and 45° (Bridgeman and Skipper, 1997). These can be interpreted as the orientations of molecules that, respectively, accept H-bonds from talc OH groups and donate H-bonds to the surface bridging oxygens. In the first water layer at a fully hydroxylated crystalline silica surface, there are three prevalent dipole orientations with φ_D = 0°, 75–105°, and 180° (based on Fig. 7 of Lee and Rossky (1994)), leading to different H-bonding environments for differently oriented water molecules. Generally, these water orientations are very similar to those for brucite, but the surface H-bonding configurations are quite different, as discussed in the next section.

In our simulations with brucite, water molecules located between 3 and 5 Å from the surface near the first minimum of O-density profile also have two different preferred orientations, as shown by their φ_D and φ_{HH} angular distributions in Figures 5d–5f (the peak positions are at 65° and 120° in (d), 80° and 180° in (e), and 95° and 180° in (f); the φ_N angular distributions are not shown). One group (type-3) has 'φ_D in the range between 90 and 180°, $\varphi_{HH}\approx$90°, and $\varphi_N\approx$20–90°, and the other (type-4) has $\varphi_D\approx$40–140°, $\varphi_{HH}\approx$0–50°, and $\varphi_N\approx$50–90°. The φ_D and φ_{HH} maxima shift for both types of molecules shift to higher angles as the distance from the surface increases from 3 to 5 Å (Figs. 5d–5f). As in the layer nearest to the surface, molecules with the two preferred orientations are intimately mixed with each other across the surface. The (type-3)/(type-4) abundance ratio varies from 2/1 at ~3 Å, to 4/1 at ~4 Å, and back to 2/1 at ~5 Å from the surface. Compared to the water molecules in the first surface layer, the distributions of the angular orientations are broader, indicating that a greater range of orientations is accessible to the molecules further away from the surface.

Although atomic density profiles (Fig. 3) show almost no variation beyond ~10 Å from the surface, small but statistically meaningful changes of the orientational distributions can be observed up to ~15 Å from the surface (Fig. 5). The changes

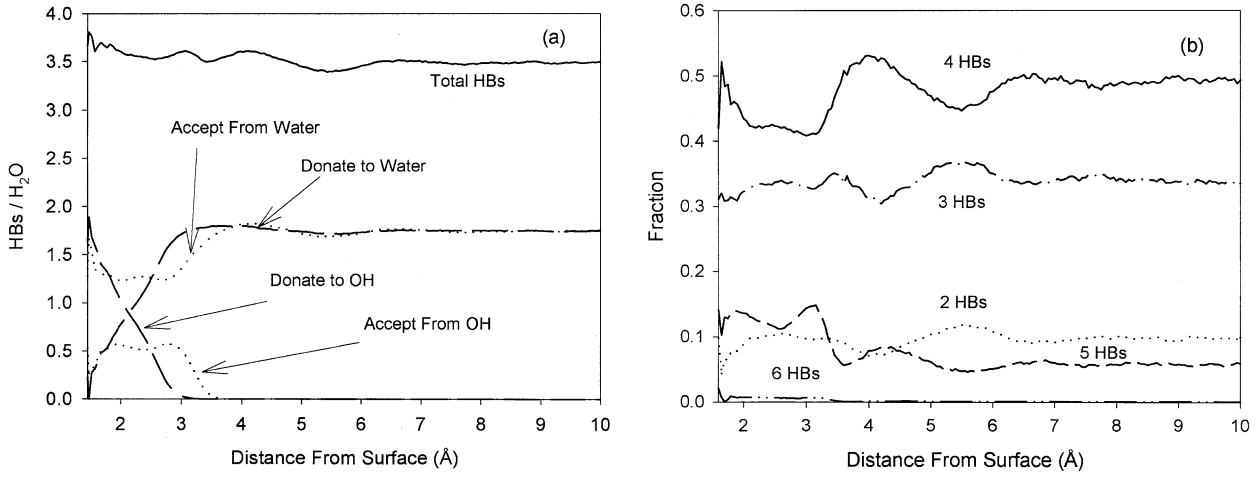

Fig. 7. (a) Variation of the average total H-bond number per water molecule, and the contributions of various H-bond types to this number with distance from the surface for the 30 Å system; (b) Variation of the average fraction of water molecules with different numbers of H-bonds with distance from the surface or the 30Å system.

in the φ_D distributions are quite similar in the two layers from 6 to 8.5 Å and from 9 to 12 Å, as shown in the left column of distributions in Figure 5. There is a single broad peak centered at 90° for water at 6.1 and 10.1 Å and three peaks centered at 0 to 30°, ~90° and 150 to 180° at 8.1 and 11.6 Å. For the φ_{HH} distributions in the same distance ranges, the orientations change continuously. There is one broad peak centered at 90° at 6.1 Å, and the intensity of this peak decreases from 6.1 to 11.6 Å, whereas the intensities of peaks at 0° and 180° increase. The breadths of the angular distributions increase with increasing distance from the surface, and deviations from random distributions decrease and require higher signal-to-noise ratios to be visible. (Note the gradual change of scale in Figures 5b–5j). These changes of angular distributions with the distance from the surface are due to adjustment of the orientations of individual water molecules to fit their local environments. These molecular orientations are effected by the surface directly at short distances from it, and indirectly at larger distances through the neighboring H_2O molecules that are, themselves, effected by the surface.

3.2. H-Bonding Network

The structuring of the near-surface water molecules described above is the result of interactions between the water molecules and the substrate, and among water molecules. H-bonding plays a significant role in developing this structure. The MD simulations show that the average number of H-bonds per H_2O molecule changes from 3.8 in the near-surface layer to 3.5 (approximately the value for bulk SPC water) at ~10 Å from the surface, and that there are significant oscillations in this value (Fig. 7a). The first layer of water molecules, which both donate and accept H-bonds with surface OH-groups, is very important in developing this interfacial H-bonding network. Molecules in the first layer that have H-atoms pointing towards the surface (type-1 molecules) have, on average, 3.6 H-bonds at ~2 Å from the surface. They accept 0.5 H-bonds from, and donate 1.0 to surface OH groups, and accept 1.3 from, and donate 0.8 to other water molecules. Those near-surface molecules that do not donate H-bonds to the surface (type-2 environments) have on average 3.6 H-bonds at ~3 Å from the surface. They accept 0.5 from, and donate none to surface OH groups, and accept 1.4 from, and donate 1.7 to other water molecules.

Computational studies for different oxide and hydroxide surfaces show quite different near-surface water structures. An interfacial water structure quite similar to that of brucite occurs at the (001) surface of portlandite, $Ca(OH)_2$, where the ability of the surface water molecules to both donate and accept H-bonds to the solid surface results in the development of an H-bonding network across the interface structurally resembling that of bulk liquid water (Kalinichev and Kirkpatrick, 2002). For water at the magnetite (001) surface Rustad et al. (2003) have recently used a potential model that allows the surface protonation state to change during the MD simulation. The results show that interfacial water molecules accept H-bonds from several surface functional groups, of which ~1/2 are $Fe^{VI}OH_2$ sites (doubly protonated O-atoms coordinated to one octahedral Fe). About 3/4 of the H-bonds donated by H_2O molecules to surface sites go to $Fe^{IV}OH$ (singly protonated O-atoms coordinated to tetrahedral Fe). These results suggest that different surface functional groups can play different roles in developing interfacial hydrogen-bonding networks. For our brucite (001) surface, only one $Mg_3{}^{VI}OH$ surface functional group is present, and these sites serve as both H-bond donors and H-bond acceptors. For a hydroxylated silica surface, Lee and Rossky (1994) have proposed two idealized structural environments for water in the first hydration layer that are significantly different than those for brucite in our results. For hydroxylated silica, one type has its dipoles oriented away from the surface and accepts one H-bond from, and donates one H-bond to surface OH groups. The other type has its dipoles oriented towards the surface and accepts one H-bond from, and donates two H-bonds to surface OH groups. These differences between water orientations at the brucite and hydroxylated silica surfaces are probably caused by the differences in the substrate surface structure. On the silica surface, the Si-OH groups are 5.0 Å apart, whereas for brucite the nearest MgOH-MgOH distance is only 3.1 Å, approximately the diameter of a water molecule. In addition, the silica surface in the model of Lee and Rossky (1994) may be less hydrophilic because the partial charges used for surface OH groups were smaller than in our calculations (−0.71 for O and 0.40 for H for silica vs. −1.105 and 0.425 for brucite).

The presence of both donating and accepting H-bond configurations at hydroxylated surfaces is not universal. For instance, the surface of the Ca-Al layered double hydroxide, $[Ca_2Al(OH)_6]Cl{\bullet}2H_2O$ (known as Friedel's salt or hydrocalumite), has a fully hydroxylated surface structure quite similar to that of $Ca(OH)_2$, but a very different surface-water structure. The positive structural layer charge of this phase and the highly distorted $Ca(OH)_6$ octahedra in the hydroxide layer prevent H-bond donation from H_2O molecules to the surface and restrict development of a fully interconnected H-bonding network across the interface (Kalinichev and Kirkpatrick, 2002).

For our brucite calculations, the number of H-bonds per water molecule oscillates with increasing distance from the surface and, on average, is somewhat greater than in bulk liquid water (Fig. 7a). At distances greater than 10 Å from the surface, H-bonding is essentially the same as in bulk SPC water, with an average of 3.5 H-bonds per molecule, 1.75 accepted and 1.75 donated (Jorgensen et al., 1983; and our unpublished simulations of bulk liquid water). Within 10 Å of the surface, the number of water molecules with 4 H-bonds varies nearly out-of-phase with the number with 2 and 3 H-bonds, and the number of molecules with 5 H-bonds controls the variation in total H-bonds (Fig. 7b). The fraction of water molecules with exactly 4 H-bonds reaches a maximum at ~4.0 Å from the surface (Fig. 7b), in the transition region with relatively low atomic density between the first two peaks of the O-atom density profiles. Similar structuring is also observed for water confined in hydroxylated silica glass pores (Gallo et al., 2002), and is in agreement with the notion that the number of water molecules with four H-bonds increases with decreasing density at liquid-like densities (Geiger and Stanley, 1982; Paulo et al., 2002).

This well-interconnected H-bonding network for brucite contrasts greatly with the water structure near hydrophobic surfaces. For instance, a water molecule participates, on average, in only ~2.5 H-bonds at the surfaces of carbon nanotubes,

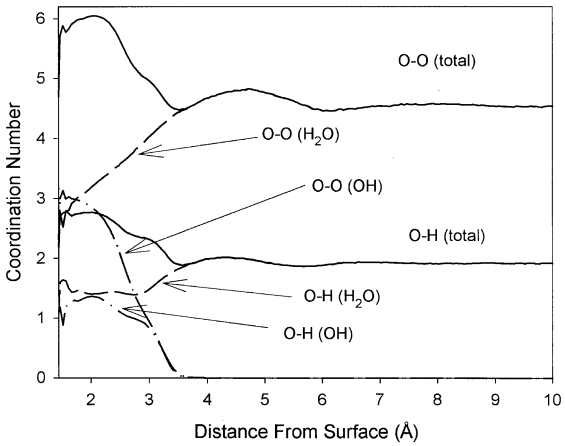

Fig. 8. Variation of the average water coordination number and the contributions to this total with distance from the surface for the 30 Å system. Cut off distances are 3.3 Å for O-O coordination and 2.45 Å for O-H coordination.

but this number increases to ~3.5 at distances greater than 4 Å from such surfaces (Gordillo and Martí, 2000).

3.3. Water Coordination

Although interactions of water molecules among themselves and with the surface OH-groups of brucite are dominated by H-bonding, the nearest neighbor (NN) coordination numbers can be greater than the number of H-bonds, and, as in bulk water, non-H-bonded NNs play an important role in defining the water structure. The water molecules at ~2.3 Å from the surface, mostly type-1 molecules, typically have 6 O-NN: 3 surface OH groups and 3 neighboring H_2O molecules (Fig. 8). These molecules are typically located above the vacant tetrahedral sites in the trioctahedral sheet, which expose a triangle of Mg-OH groups on the surface. The 3 NN water molecules occur at three of the four vertices of a distorted tetrahedron. The water molecules at ~3.0 Å from the surface, mostly type-2 molecules, have, on average, 5 O-NNs: 1 OH and 4 H_2O molecules. Three of these 4 water molecules are arranged at three vertices of a distorted tetrahedron, and the MgOH-group is at the fourth vertex. The fifth water molecule occurs close to one face of the tetrahedron and behaves like a typical interstitial molecule in bulk water (Bagchi et al., 1997; Kalinichev et al., 1999). Beyond ~3.5 Å from the surface, the NN coordination is generally similar to that of bulk liquid water, which has 4.4 nearest neighbors in our MD simulations at the same temperature and density. There is a slight increase in the coordination number in the region between 3.5 to 6.0 Å from the surface, which corresponds to the second maximum in the O-atomic density profile.

The results presented here show that the H-bonding and NN coordination of water at the brucite surface do not resemble those of water at reduced temperatures, as proposed for water confined in Vycor glass and silica gel based on neutron diffraction studies (Dore, 2000; Bellissent-Funel, 2001). This is shown not just by the sixfold coordination near the surface, which does not occur at ambient pressure, but also in the relationships between the NN coordination and the number of H-bonds. At distances greater than ~6 Å from the brucite surface, the NN coordination is ~4.4, which is ~0.9 greater than the number of H-bonds. Closer to the surface the number of NNs is as much as 2.2 greater than the number of H-bonds. The number of H-bonds and the NN coordination also both increase with decreasing distance from the surface, but the coordination number increases faster. In contrast, cooling of bulk liquid water causes the average number of H-bonds to increase with the NN coordination remaining more or less constant (Rapaport, 1983; Paulo et al., 2002). This change reaches its limit of H-bonds/NN = 1 in the stable 1-atm crystalline phase, ice Ih (Eisenberg and Kauzmann, 1969). Thus, the structural changes of water with decreasing temperature can be understood as an approach to an ideal tetrahedral NN coordination and H-bonding network. In addition, cooling causes the distributions of H-bond angles and lengths to become narrower, the mean H-bond angle (angle β in Fig. 2) to decrease, and the second-neighbor spatial correlations that are lost at higher temperature to be restored to a more ideal (ice-like) geometry (Modig et al., 2003). MD simulations for water confined in hydrated Vycor pores (Gallo et al., 2002) and for water confined in carbon nanotubes (Gordillo and Martí, 2000) also show that the ice Ih-like NN and H-bond geometry of bulk water is destroyed near these surfaces.

The structure of the first layer of water at the brucite surface does share some similarities with those of liquid water at elevated pressure and high-pressure ice phases. With increasing pressure, the average NN coordination for liquid water increases more rapidly than the average number of H-bonds (Kalinichev et al., 1999; Paulo et al., 2002), and the structural changes can best be interpreted in terms of an increasing number of interstitial (non-H-bonded) water molecules (Bagchi et al., 1997; Kalinichev et al., 1999; Saitta and Datchi, 2003). In the crystalline ice phases, there are always four H-bonded nearest neighbors at intermolecular distances of 2.7 to 2.9 Å, but the number and intermolecular distances of the non-H-bonded molecules are different for different phases. There are zero non-H-bonded molecules in ice Ih (stable up to 0.3 GPa), 3.75 at 3.1 to 3.3 Å in ice IV (a metastable phase at 0.4 to 0.55 GPa, Engelhardt and Kamb, 1981), and 4 at 2.74 Å in ice VIII (stable above 2.1 GPa, Kuhs et al., 1984). The latter distance is shorter than the H-bond distance (2.88 Å) in that phase, paralleling a similar trend for liquid water under pressure (Schwegler et al., 2000). At the brucite surface, the coordination number is 5 or 6, and number of H-bonds is ~3.8, qualitatively following the trends for liquid water and the crystalline phases with increasing pressure. However, the surface contributes at least half of these additional NNs for type-1 molecules, and the average density of the near-surface water, up to the first minimum of the O-density profile, is slightly less than for bulk water at ambient conditions.

The differences just described are also reflected in the differences between the two-dimensional RDFs of water at the brucite surface and the RDFs of water at high pressure or low temperature. For bulk liquid water, the widths of the first and second peaks in the O-O RDFs decrease with decreasing temperature (Schwegler et al., 2000; Soper, 2000), whereas this does not occur for water on brucite (001) as a function of distance from the surface (Fig. 9). With increasing pressure for liquid water, the O-O RDF intensity at ~3.2 Å increases (Soper, 2000), reflecting the larger NN coordination number, the intensity at ~4.5Å decreases, and the intensity at ~5.3 increases

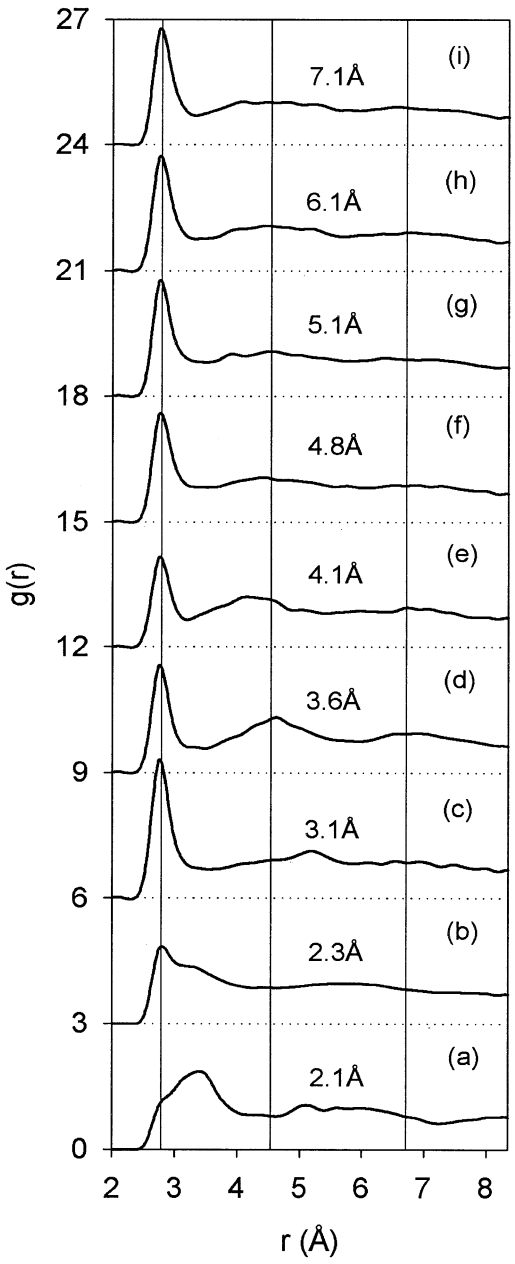

Fig. 9. Two-dimensional water O-O radial distribution functions calculated for the indicated distances from the surface for the 15 Å system. Two-dimensional RDFs were calculated in 0.2 Å slices along the brucite [001] direction. The curves are displaced 3.0 Å vertically to avoid overlap. The vertical lines are at 2.8, 4.5, and 6.7 Å from the surface, corresponding to the first three peaks in the three-dimensional RDF of SPC water at ambient conditions.

(Schwegler et al., 2000). This is very similar to the two-dimensional RDF for water at ~3Å from the brucite surfaces, except for the peak at 3.2 Å, which does not occur (Fig. 9).

3.4. Structural Organization of Surface Water on Brucite

It is well known that liquid water is significantly ordered at solid surfaces (Packer, 1977; Nandi et al., 2000; Michot et al., 2002), but the MD results here show that this surface-induced structural ordering can be quite different and more complicated than commonly thought. For instance, the description of the interfacial water structure at the brucite surface as ice-like is misleading, as discussed above. For water on brucite, there are three regions at progressively increasing distances from the surface with different degrees of ordering: a well organized first layer, a transition region of lower-than-average atomic density from 3 Å to 5 Å from the surface, and less well-ordered ordered layers extending to as far as 15 Å from the surface.

The organization of the first layer is best illustrated by the atomic density contour maps for the O-atoms of H_2O molecules, located in the first maximum in the atomic density profile between 1.85 and 3.45 Å from the surface (Fig. 10). The type-1 water molecules are preferentially located above the vacant tetrahedral sites of the trioctahedral sheet (triangles formed by surface OH-groups; Fig. 10a). They form a reasonably well-ordered and dynamically averaged two-dimensional hexagonal

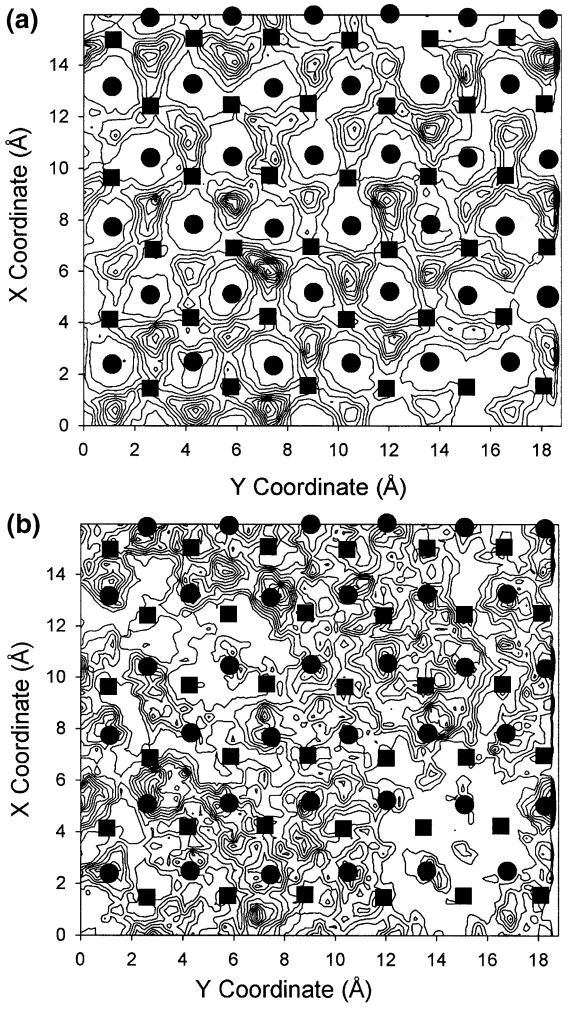

Fig. 10. Typical atomic density maps for oxygen of water in the first layer. The filled squares and circles are surface Mg and O atoms respectively, and the thin lines are contour maps for water oxygen atoms. The top figure is for water molecules with φ_D greater than 90° (Type-1 environment), and the bottom figure is for water molecules with φ_D less than 90° (Type-2 environment).

arrangement with a quasi (1 × 1) superstructure that reflects the underlying brucite structure. There appear to be four local potential energy minima. One of these is at the center of the triangle, and three are nearly at the middle of the line connecting two surface OH sites. The surface water molecules spend on average ~1/2 of the time at the center, where they accept only 1 HB, and 1/6 of the time at each of the other sites, where they donate one and accept one HB. This site hopping, libration, and formation and breaking of HBs, results in the computed average of 1.5 HBs with surface OH groups discussed above.

The two-dimensional RDF, which probes the intermolecular structure in the plane parallel to the surface, confirms this lattice-like arrangement (Fig. 9). If the water molecules had adapted the surface lattice structure perfectly, the first four peaks of their two-dimensional RDF would occur at 3.1, 5.4, 6.3, and 8.3 Å, corresponding to the [100], [110], [200], and [210] dimensions of the brucite lattice, as calculated from the two-dimensional RDF of the surface O-atoms of the brucite. Because of the triangular distributions of the water molecules shown in Figure 10, these peaks become broader and shift to different values, but they are clearly present. The distributions of the order parameter, *q*, which measures the deviation of the local structure from the ideal tetrahedrality of the ice Ih lattice, show that the structure of this group of molecules is very different from that of ice Ih, with a large fraction of the molecules having *q*-values less than 0.5 (Fig. 11a–11d). These values are consistent with the 6 NN coordination of these molecules.

The type-2 water molecules in the first layer (those with their dipoles oriented away from the surface) are preferentially located above the OH groups, but their distribution is much less ordered than for the type-1 molecules (Fig. 10b). Only half of the type-2 molecules accept one H-bond from surface OH groups at any instant. The distributions of the order parameter, *q*, show that the intensity of the distribution near 0.5 is greater than at 0.8, in contrast to bulk water, which has greater intensity near 0.8. These low *q*-values are consistent with the average 5 NN coordination of these molecules. On average, there are 15.1 type-1 water molecules and 12.4 type-2 water molecules (totaling 27.5) in the first layer of water molecules for each 36 surface OH lattice sites of brucite. This lattice-like two-dimensional distribution for water molecules on surfaces is not unique to brucite. It is known to occur in the first layer of water in MD simulations at the NaCl (100) surface, where the two-dimensional structure reflects the underlying NaCl crystal structure (Stöckelmann and Hentschke, 1999).

For brucite, this surface structure also explains the position of the first maximum in the O-atomic density profile, which is 2.45 Å from the surface (Fig. 3). If all the water molecules were located directly above the vacant tetrahedral sites, the O-density maximum should be ~2.1 Å above surface, assuming a distance of 2.8 Å between O-of-OH and O-of-water, which is the position of the first peak of O-O RDF in bulk water, and a distance of 3.1 Å between the NN OH groups on the surface, which is the value in bulk brucite. The 0.4 Å increase arises because of the population of molecules that occur above the surface OH-sites (type-2 molecules). This configuration is different than at the surfaces of other phases, and evidence from several studies indicates that the position of the first peak of the

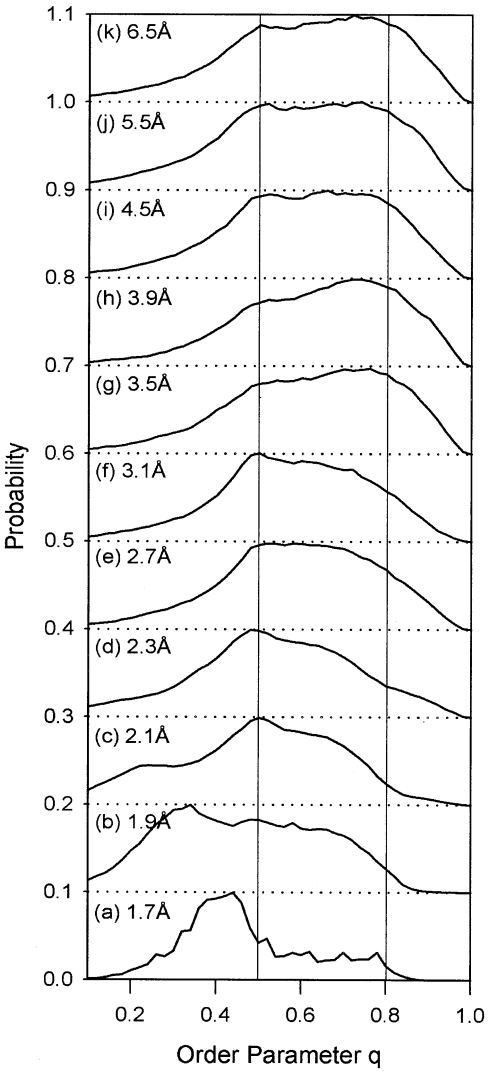

Fig. 11. Distributions of the orientation order parameter, *q*, in 0.05 Å slices along the brucite [001] direction in the 12 Å system for the indicated distances from the surface.

O-density profile is substrate-specific. For instance, water at the (001) mica surface is located at 1.3 Å from the surface, due to the water molecules occupying the ditrigonal cavities (Cheng et al., 2001; Park and Sposito, 2002). On the non-hydroxylated MgO (001) surface, they are located ~2.2Å from the surface, due to H-bond donation to the surface O atoms (McCarthy, et al., 1996).

In the low-density transition region between 3 Å and 5 Å from the brucite surface, the first peak in the two-dimensional O-O RDF is always at ~2.8 Å, the same as in bulk water, but the second peak changes continuously from 5.5 Å (a brucite lattice-like value) at 3 Å from the surface, to 4.5 Å (a bulk water-like value), ~5 Å from the surface. This interval is, thus, the transition region from the near-surface layer with a structure largely controlled by the substrate to a more or less bulk water-like structure. This transition occurs by gradual adjustment of the second neighbor configuration in a distorted, but locally tetrahedral structure. Water molecules located 4 Å from

surface in this transition region have the largest average orientational order parameter ($q = 0.65$), reflecting a degree of ice Ih-like tetrahedral ordering greater than in even bulk water. This is also shown by the two-dimensional RDFs, in which the first-neighbor peak is depressed and the second-neighbor peak enhanced (Fig. 9e). The distribution of order parameters at this distance from the surface (Fig. 11h) is bimodal with intensity near $q = 0.8$ greater than in bulk liquid water under ambient conditions (essentially the same as in Figure 11k; see Errington and Debenedetti, 2001). The $q = 0.8$ peak represents the H_2O molecules with an ordered ice-like local structure, and the $q = 0.5$ peak represents the H_2O molecules with nearest neighbor configurations distorted by interstitial molecules (Bagchi et al., 1997; Errington and Debenedetti, 2001; Saitta and Datchi, 2003). The reduced intensity of the $q = 0.5$ peak at 4 Å from the brucite surface thus indicates that more molecules at this distance from the surface adapt a disordered ice-like structure, and that there are fewer interstitial water molecules than in bulk water.

The structure of water in the region between 5 and 15 Å from the surface, that contains O-density profile maxima at 5.05, 6.25, 9.05 Å, is somewhat more ordered than bulk water, but less ordered than the first surface layer. The atomic density map for the oxygens of H_2O molecules in the second maximum in the density profile (3.45 to 5.65 Å from the surface) shows no clearly preferred sites. At these distances from the surface, the atomic density profiles (Fig. 3), the orientational order parameter distributions (Fig. 11), H-bond numbers (Fig. 7), coordination numbers (Fig. 8), and distributions of molecular orientations (Figs. 4 and 5) vary only slightly from their bulk values. The two-dimensional RDFs (Fig. 9h and 9i) also show no additional ordering relative to the bulk structure. Further from the surface, all computed structural parameters are indistinguishable from their values for bulk liquid water.

4. CONCLUSIONS AND IMPLICATIONS

The MD simulations of one-dimensional nano-confinement of liquid water by two surfaces of brucite presented here provide a greatly increased, atomistically detailed understanding of surface effects on the spatial variation in the structural ordering, hydrogen bond organization, and local density of H_2O molecules near the surfaces of electrostatically neutral metal hydroxides. Both H-bond donation to the surface oxygen atoms and H-bond acceptance from the surface OH-groups in the first surface layer of H_2O molecules play key roles in controlling the structure. The oxygen and hydrogen atomic densities and H_2O dipole orientations vary significantly with distance from the surface and deviate from the corresponding structural properties of bulk water to distances as large as 15 Å (~5 molecular water layers) from the surface. The water molecules in the first layer at ~2.45 Å from the surface have a two-dimensional hexagonal arrangement in the plane parallel to the surface, reflecting the brucite structure. They have total nearest neighbor coordinations by surface OH-groups and water molecules of 5 or 6 and are significantly limited in their position and orientation by the surface. The greatest degree of the tetrahedral (ice-like) ordering occurs at ~4 Å from the surface. The translational and orientational ordering of H_2O molecules in layers further from the surface become progressively more similar to those of bulk liquid water. The computed structure of the interfacial water results from a combination of "hard wall" (geometric and confinement) effects, highly directional H-bonding, and thermal motion. This structure shares some similarities with that of water under higher pressure, but does not resemble that of bulk water at ambient conditions or at elevated or reduced temperature.

These structural changes can be described as a gradual decrease of substrate-induced ordering and a gradual broadening of the ranges of orientational and translational coordinates accessible to the interfacial water molecules. The near-surface translational ordering extends to ~5 Å from the surface, density effects to ~10 Å, and orientational effects to ~15 Å. The substrate-dominated structure of the first water layer and the ice Ih-like structure, centered, respectively, at ~2 and 4 Å from the surface, may be detectable in synchrotron-based X-ray adsorption measurements (e.g., Myneni et al., 2002), thus allowing experimental testing of the computational results discussed here. These structures may also persist at lower temperatures, even below the freezing temperature of interfacial water. At even lower temperatures, these layers might freeze to a new form of ice.

Detailed atomic-scale knowledge of the structure and properties of aqueous interfaces with minerals, such as those obtained here, is crucial to the quantitative understanding and prediction of many important geochemical and environmental phenomena, including mineral dissolution/precipitation, surface sorption of aqueous species, and solute transport mechanisms in many environments (e.g., Hochella and White, 1990; Brown et al., 1999; Brown, 2001). Recent experimental studies have provided improved atomic-scale understanding of the interfacial water structure and atomic density oscillations in water adjacent to mineral surfaces of calcite, barite, muscovite, and K-feldspar (Fenter et al., 2000a; Fenter et al., 2000b; Cheng et al., 2001; Schlegel et al., 2002). These X-ray reflectivity measurements have demonstrated that the degree of ordering at mineral-water interfaces depends sensitively on the mineral structure and composition (Fenter et al., 2003). Such experimental studies, however, usually require nearly perfect macroscopic crystal surfaces, and many geochemically and environmentally important minerals, including hydroxides, oxyhydroxides, clays, and related phases, and are typically fine grained and/or poorly crystalline.

In addition, X-ray reflectivity probes integrated electron density at the surface and, thus, sometimes has difficulty distinguishing between water and other solution species. It is also relatively insensitive to the positions of hydrogen atoms and, thus, to the structure of the H-bond network. Neutron scattering can effectively probe the H-bonding in some cases (e.g., Skipper et al., 2000). In many important cases, however, molecular-scale computational modeling can provide significant, and otherwise unobtainable, understanding of the structures and properties of the aqueous interfaces. Metal hydroxide surfaces are of great importance geochemically (Refson et al., 1995; Liu et al., 1998; Brown et al., 1999). Brucite is a prototypical hydroxide, and the results presented here are, thus, an important reference for future studies.

The classical MD approach used here does not include quantum phenomena, and thus does not allow analysis of such processes as proton transfer among water molecules or between

brucite and water (e.g., Horita et al., 1999). Nonetheless, it is now well established that classical methods using relatively simple empirical potentials, in which intermolecular H-bonding arises due to electrostatic interactions among partially charged atoms, provide a good quantitative picture of H-bonding in water over a wide range of thermodynamic conditions, from ambient to hydrothermal (e.g., Kalinichev, 2001; Guillot, 2002). This should also hold true for the interaction of water with many oxide and hydroxide substrates, because the covalent and electrostatic bonding mechanisms are the same in both cases.

Acknowledgments—This research was supported by DOE Basic Energy Sciences Grant DEFGO2−00ER-15028. Computation was partially supported by the National Computational Science Alliance (Grant EAR 990003N) and utilized NCSA SGI/CRAY Origin 2000 computers and Cerius2−4.6 software package from Accelrys. J. Wang also acknowledges a fellowship from the University of Illinois at Urbana-Champaign. Fruitful discussions with R. T. Cygan about forcefield parameterization and J. D. Kubicki about the structure of aqueous solutions at interfaces are most gratefully acknowledged.

Associate editor: U. Becker

REFERENCES

Abraham F. F. (1978) The interfacial density profile of a Lennard-Jones fluid in contact with a (100) Lennard-Jones wall and its relationship to idealized fluid/wall systems: A Monte Carlo simulation. *J. Chem. Phys.* **68,** 3713–3716.

Allen M. P. and Tildesley D. J. (1987) *Computer Simulation of Liquids*. Clarendon Press.

Bagchi K., Balasubramanian S., and Klein M. L. (1997) The effects of pressure on structure and dynamical properties of associated liquids: Molecular dynamics calculations for the extended simple point charge model of water. *J. Chem. Phys.* **107,** 8561−8567.

Bellissent-Funel M-C. (2001) Structure of confined water. *J. Phys.: Condens. Matter.* **13,** 9165–9177.

Bellissent-Funel M-C. (2002) Water near hydrophilic surfaces. *J. Mol. Liq.* **96-97,** 287–304.

Berendsen H. J. C., Postma J. P. M., van Gunsteren W. F., and Hermans J. (1981) Interaction models for water in relation to protein hydration. In *Intermolecular Forces* (ed. B. Pullman), p. 331, Riedel: Dordrecht.

Bridgeman C. H. and Skipper N. T. (1997) A Monte Carlo study of water at an uncharged clay surface. *J. Phys.: Condens. Matter.* **9,** 4081−4087.

Brown G. E., Jr. (2001) How minerals react with water. *Science* **294,** 67–70.

Brown G. E., Jr, Henrich V. E., Casey W. H., Clark D. L., Eggleston C., Felmy A., Goodman D. W., Grätzel M., Maciel G., McCarthy M. I., Nealson K. H., Sverjensky D. A., Toney M. F., and Zachara J. M. (1999) Metal oxide surfaces and their interactions with aqueous solutions and microbial organisms. *Chem. Rev.* **99,** 77–174.

Chau P.-L. and Hardwick A. J. (1998) A new order parameter for tetrahedral configurations. *Mol. Phys.* **93,** 511–518.

Cheng L., Fenter P., Nagy K. L., Schlegel M. L., and Sturchio N. C. (2001) Molecular-scale density oscillations in water adjacent to a mica surface. *Phys. Rev. Lett.* **87,** 156103-4.

Cygan R. T. (2001) Molecular modeling in mineralogy and geochemistry. *Rev. Mineral. Geochem.* **42,** 1–35.

Cygan R. T., Liang J-J., and Kalinichev A. G. (2004) Molecular models of hydroxide, oxyhydroxide, and clay phases and the development of a general forcefield. *J. Phys. Chem. B.* **108,** 1255–1266.

Desgranges L., Calvarin G., and Chevrier G. (1996) Interlayer interactions in $M(OH)_2$: A neutron diffraction study of $Mg(OH)_2$. *Act Cryst. B.* **52,** 82−86.

Dore J. (2000) Structural studies of water in confined geometry by neutron diffraction. *Chem. Phys.* **258,** 327–347.

Drever J. I. (1997) *The Geochemistry of Natural Waters-Surface and Groundwater Environments*. Third edition, Prentice Hall.

Eisenberg D. and Kauzmann W. (1969) *The Structure and Properties of Water*. p. 296. Oxford University Press.

Engelhardt H. and Kamb B. (1981) Structure of ice IV, a metastable high-pressure phase. *J. Chem. Phys.* **75,** 5887–5899.

Errington J. R. and Debenedetti P. G. (2001) Relationship between structural order and the anomalies of liquid water. *Nature* **409,** 318–321.

Fenter P., Teng H., Geissbuhler P., Hanchar J. M., Nagy K. L., and Sturchio N. C. (2000a) Atomic-scale structure of the orthoclase (001)-water interface measured with high-resolution X-ray reflectivity. *Geochim. Cosmochim. Acta* **64,** 3663–3673.

Fenter P., Geissbuhler P., DiMasi E., Srajer G., Sorensen L. B., and Sturchio N. C. (2000b) Surface speciation of calcite observed in situ by high-resolution X-ray reflectivity. *Geochim. Cosmochim. Acta* **64,** 1221–1228.

Fenter P., Cheng L., Park C., Zhang Z., and Sturchio N. C. (2003) Structure of the orthoclase (001)- and (010)-water interfaces by high-resolution X-ray reflectivity. *Geochim. Cosmochim. Acta* **67,** 4267−4275.

Fouzri A., Dorbez-Sridi R., and Oumezzine M. (2002) Water confined in silica gel and in vycor glass at low and room temperature, x-ray diffraction study. *J. Chem. Phys.* **116,** 791–797.

Gallo P., Rapinesi M., and Rovere M. (2002) Confined water in the low hydration regime. *J. Chem. Phys.* **117,** 369−375.

Geiger A. and Stanley H. U. (1982) Low-density "patches" in the hydrogen-bond network of liquid water: Evidence from molecular-dynamics computer simulations. *Phys. Rev. Lett.* **49,** 1749−1752.

Geissler P. L., Dellago C., Chandler D., Hutter J., and Parrinello M. (2001) Autoionization in liquid water. *Science* **291,** 2121–2124.

Greathouse J. A., Refson K., and Sposito G. (2000) Molecular dynamics simulation of water mobility in magnesium-smectite hydrates. *J. Am. Chem. Soc.* **122,** 11459−11464.

Gorbaty Y. E. and Kalinichev A. G. (1995) Hydrogen bonding in supercritical water. 1. Experimental results. *J. Phys. Chem.* **99,** 5336−5340.

Gordillo M. C. and Martí J. (2000) H-bond structure of liquid water confined in nanotubes. *Chem. Phys. Lett.* **329,** 341–345.

Guillot B. (2002) A reappraisal of what we have learnt during three decades of computer simulations on water. *J. Mol. Liq.* **101,** 219−260.

Hartnig C., Witschel W., and Spohr E. (1998) Molecular dynamics study of the structure and dynamics of water in cylindrical pores. *J. Phys. Chem.* **102,** 1241–1249.

Head-Gordon T. and Hura G. (2002) Water Structure from Scattering Experiments and Simulation. *Chem. Rev.* **102,** 2651–2670.

Hochella M. F., Jr. and White A. F. (1990) Mineral-water interaction geochemistry: An overview. *Rev. Mineral.* **23,** 1–16.

Horita J., Driesner T., and Cole D. R. (1999) Pressure effect on hydrogen isotope fractionation between brucite and water at elevated temperatures. *Science* **286,** 1545–1547.

Israelachvili J. N. and Pashley R. M. (1983) Molecular laying of water at surfaces and origin of repulsive hydration forces. *Nature* **306,** 249–250.

Israelachvili J. N. and Wennerström H. (1996) Role of hydration and water structure in biological and colloidal interactions. *Nature* **379,** 219–225.

Jorgensen W. L., Chandrasekhar J., Madura J. F., Impey R. W., and Klein M. L. (1983) Comparison of simple potential functions for simulating liquid water. *J. Chem. Phys.* **79,** 926–935.

Kagunya W. W. (1996) Properties of water adsorbed in anionic clays: A neutron scattering study. *J. Phys. Chem.* **100,** 327–330.

Kalinichev A. G. (2001) Molecular simulations of liquid and supercritical water: Thermodynamics, structure, and hydrogen bonding. *Rev. Mineral. Geochem.* **42,** 83–130.

Kalinichev A. G. and Kirkpatrick R. J. (2002) Molecular dynamics modeling of chloride binding to the surfaces of Ca hydroxide, hydrated Ca-aluminate and Ca-silicate phases. *Chem. Mater.* **14,** 3539–3549.

Kalinichev A. G., Gorbaty Y. E., and Okhulkov A. V. (1999) Structure and H-bonding of liquid water at high hydrostatic pressure: Monte

Carlo NPT-ensemble simulations up to 10 kbar. *J. Mol. Liq.* **82,** 57–72.

Kalinichev A. G., Kirkpatrick R. J., and Cygan R. T. (2000) Molecular modeling of the structure and dynamics of the interlayer and surface species of mixed-metal layered hydroxides: chloride and water in hydrocalumite (Friedel's salt). *Am. Miner.* **85,** 1046–1052.

Kirkpatrick R. J., Kalinichev A. G., Wang J., Hou X., and Amonette J. E. (2004) Molecular modeling of the vibrational spectra of interlayer and surface species of layered double hydroxides. In *The Application of Vibrational Spectroscopy to Clay Minerals and Layered Double Hydroxides, CMS Workshop Lectures*, vol. 13 (ed. J. T. Kloprogge). *The Clay Minerals Society*, Aurora, CO, pp. 239–285.

Kuhs W. F., Finney J. L., Vettier C., and Bliss D. V. (1984) Structure and hydrogen ordering in ice VI, VII, and VIII by neutron powder diffraction. *J. Chem. Phys.* **81,** 3612–3623.

Lee S. H. and Rossky P. J. (1994) A comparison of the structure and dynamics of liquid water at hydrophobic and hydrophilic surface-a molecular dynamics simulation study. *J. Chem. Phys.* **100,** 3334–3345.

Liu P., Kendelewicz T., and Brown G. E., Jr. (1998) Reaction of water with MgO (001) surfaces. Part II: Synchrotron photoemission studies of defective surfaces. *Surf. Sci.* **412/413,** 315–332.

Luzar A. (2000) Resolving the H-bond dynamics conundrum. *J. Chem. Phys.* **113,** 10663–10675.

McCarthy M. I., Schenter G. K., Scamehorn C. A., and Nicholas J. B. (1996) Structure and dynamics of the water/MgO interface. *J. Phys. Chem.* **100,** 16989–16995.

Michot L. J., Villiéras F., Francois M., Bihannic I., Pelletier M., and Cases J-M. (2002) Water organization at the solid-aqueous solution. *C. R. Geoscience* **334,** 611–631.

Modig K., Pfrommer B. G., and Halle B. (2003) Temperature-dependent hydrogen-bond geometry in liquid water. *Phys. Rev. Lett.* **90,** 075502-4.

Myneni S., Luo Y., Näslund L., Å., Cavalleri M., Ojamäe L., Ogasawara H., Pelmenschikov A., Wernet Ph., Väterlein P., Heske C., Hussain Z., Pettersson L. G. M., and Nilsson A. (2002) Spectroscopic probing of local hydrogen-bonding structure in liquid water. *J. Phys.: Condens. Matter.* **14,** L213–L219.

Nandi N., Bhattacharyya K., and Bagchi B. (2000) Dielectric relaxation and solvation dynamics of water in complex chemical and biological systems. *Chem. Rev.* **100,** 2013–2045.

Packer K. J. (1977) The dynamics of water in heterogeneous systems. *Phil. Trans. Royal Soc. Lond. B.* **278,** 59–87.

Park S-H. and Sposito G. (2002) Structure of water adsorbed on a mica surface. *Phys. Rev. Lett.* **89,** 085501-3.

Paulo A. N., Starr F. W., Barbosa M. C., and Stanley H. E. (2002) Relation between structure and dynamical anomalies in supercooled water. *Phys. A.* **314,** 470–476.

Poole P. H., Sciortino F., Grande T., Stanley H. E., and Angell C. A. (1994) Effect of H-bonds on the thermodynamic behavior of liquid water. *Phys. Rev. Lett.* **73,** 1632–1635.

Raviv U., Laurat P., and Klein J. (2001) Fluidity of water confined to subnanometre films. *Nature* **413,** 51–54.

Rapaport D. C. (1983) H-bonds in water: Network organization and lifetimes. *Mol. Phys.* **50,** 1151–1162.

Refson K., Wogelius R. A., and Fraser D. G. (1995) Water chemisorption and reconstruction of the MgO surface. *Phys. Rev. B.* **52,** 10823–10826.

Rustad J. R., Felmy A. R., and Bylaska E. J. (2003) Molecular simulation of the magnetite-water interface. *Geochim. Cosmochim. Acta* **67,** 1001–1016.

Saitta A. M. and Datchi F. (2003) Structure and phase diagram of high density water: The role of interstitial molecules. *Phys. Rev. E.* **67,** 020201-4.

Sakuma H., Tsuchiya T., Kawamura K., and Otsuki K. (2003) Large self-diffusion of water on brucite surface by ab initio potential energy surface and molecular dynamics simulations. *Surf. Sci.* **536,** L396–402.

Schlegel M. L., Nagy K. L., Fenter P., and Sturchio N. C. (2002) Structures of quartz (1010)- and (1011)-water interfaces determined by X-ray reflectivity and atomic force microscopy of natural growth surfaces. *Geochim. Cosmochim. Acta* **66,** 3037–3054.

Schwegler E., Galli G., and Gygi F. (2000) Water under pressure. *Phys. Rev. Lett.* **84,** 2429–2432.

Skipper N. T., Williams G. D., de Siqueira A. V. C., Lobban C., and Soper A. K. (2000) Time-of-flight neutron diffraction studies of clay-fluid interactions under basin conditions. *Clay Minerals* **35,** 283–290.

Smirnov K. S. and Bougeard D. (1999) A molecular dynamics study of structure and short-time dynamics of water in kaolinite. *J. Phys. Chem. B.* **103,** 5266–5273.

Soper A. K. (2000) The radial distribution functions of water and ice from 220 to 673K and at pressure up to 400 MPa. *Chem. Phys.* **258,** 121–137.

Spohr E., Hartnig C., Gallo P., and Rovere M. (1999) Water in porous glasses. A computer simulation study. *J. Mol. Liq.* **80,** 165–178.

Stöckelmann E. and Hentschke R. (1999) A molecular-dynamics simulation study of water on NaCl(001) using a polarizable model. *J. Chem. Phys.* **110,** 12097–12107.

Teixeira J., Bellissent-Funelt M-C., and Chen S-H. (1990) Dynamics of water studied by neutron scattering. *J. Phys.: Condens. Matter.* **2,** SA105–SA108.

Teleman O., Jönsson B., and Engström S. (1987) A molecular dynamics simulation of a water model with intramolecular degrees of freedom. *Mol. Phys.* **60,** 193–203.

Teschke O., Ceotto G., and de Souza E. F. (2001) Interfacial water dielectric-permittivity-profile measurements using atomic force microscopy. *Phys. Rev. E.* **64,** 011605-10.

Wang J., Kalinichev A. G., Kirkpatrick R. J., and Hou X. (2001) Molecular modeling of the structure and energetics of hydrotalcite hydration. *Chem. Mater.* **13,** 145–150.

Wang J., Kalinichev A. G., Amonette J. E., and Kirkpatrick R. J. (2003) Interlayer structure and dynamics of Cl-hydrotalcite: Far infrared spectroscopy and molecular dynamics modeling. *Am. Miner.* **88,** 398–409.

Yu C.-J., Richter A. G., Datta A., Durbin M. K., and Dutta P. (1999) Observation of molecular layering in thin liquid films using X-ray reflectivity. *Phys. Rev. Lett.* **82,** 2326–2329.

Zhu Y. and Granick S. (2001) Viscosity of interfacial water. *Phys. Rev. Lett.* **87,** 096104-4.